J Pharmacol Sci **126**, 216 – 229 (2014)

Journal of Pharmacological Sciences

Full Paper

Involvement of the Nrf2 Pathway in the Regulation of Pterostilbene-Induced Apoptosis in HeLa Cells via ER Stress

Bo Zhang[1], Xiao-Qin Wang[1,*], Han-Yin Chen[1], and Bin-Hua Liu[2]

[1]*Key Laboratory of Xinjiang Endemic Phytomedicine Resources, Ministry of Education, Pharmacology Department, School of Pharmacy, Shihezi University, Shihezi 832002, China*
[2]*Medical and Nursing School, Chendu University, Chendu 610106, China*

Received February 6, 2014; Accepted August 17, 2014

Abstract. Among the various cancer cell lines, HeLa cells were found to be sensitive to pterostilbene (Pte), a compound that is enriched in small fruits such as grapes and berries. However, the mechanism involved in the cytotoxicity of Pte has not been fully characterized. Using biochemical and free radical biological experiments in vitro, we identified the pro-apoptotic profiles of Pte and evaluated the level of redox stress–triggered ER stress during HeLa cell apoptosis. The data showed a strong dose–response relationship between Pte exposure and the characteristics of HeLa apoptosis in terms of changes in apoptotic morphology, DNA fragmentation, and activated caspases in the intrinsic apoptotic pathway. During drug exposure, alterations in the intracellular redox homeostasis that favor oxidation were necessary to cause ER stress–related apoptosis, as demonstrated by enzymatic and non-enzymatic redox modulators. A statistically significant and dose-dependent increase ($P < 0.05$) was found with regard to the unique expression levels of Nrf2/ARE downstream target genes in HeLa cells undergoing late apoptosis, levels that were restored with anti-oxidant application with the Pte treatment. Our research demonstrated that Pte trigged ER stress by redox homeostasis imbalance, which was negatively regulated by a following activation of Nrf2.
[Supplementary Figure and Table: available only at http://dx.doi.org/10.1254/jphs.14028FP]

Keywords: apoptosis, ER-stress, HeLa cell, pterostilbene, redox homeostasis

Introduction

Cervical cancer is the second most common and the fifth deadliest cancer in women (1). Approximately 80% of cervical cancers occur in developing countries (2), with 409,000 new cases diagnosed annually and 234,000 deaths (3). Although new medical technologies, such as HPV vaccines and radiation therapy, have been proven to be successful for controlling cervical cancer, they are unaffordable in many medium- and low-income areas due to their high costs (4). However, evidence regarding the application of chemotherapeutical agents as treatment/preventative methods shows both increased affordability and better outcomes (5).

*Corresponding author. wangxq5166@sina.com
Published online in J-STAGE on October 21, 2014
doi: 10.1254/jphs.14028FP

The basic principle of a cancer chemoprevention strategy is to inhibit, reverse, or retard the process of multistage carcinogenesis by using defined nontoxic chemical substances (6, 7). However, the current chemopreventive regimens, such as cisplatin, paclitaxel, gemcitabine, and 5-flourouracil, are questionable for their undesirable side effects after long-term administration (5, 8). Therefore, cancer chemoprevention studies in cervical cancer using natural chemopreventive agents from food, which are relatively safe, have become an area of great interest (9).

Within the context of cervical cancer chemoprevention by natural products, intrinsic apoptosis via the endoplasmic reticulum (ER) due to increased oxidative stress in cervical cancer cells may represent a therapeutic target. Indeed, early encouraging results from in vitro studies and clinical trials suggest that reactive oxygen species (ROS) modulation therapy in patients warrants

further investigation, particularly with regard to the signal transduction pathways involved in the intracellular thiol redox environment (10, 11). Reduced glutathione (GSH) is the most abundant intracellular thiol and is therefore the major regulator of intracellular redox homeostasis (12). Other anti-oxidative compensators of redox homeostasis are mainly modulated by the redox-sensitive transcription factor nuclear factor erythroid-2-related factor-2 (Nrf2), which interacts with the anti-oxidant response element (ARE) located in the promoter region of genes encoding anti-oxidant or detoxifying enzymes (13). Nrf2 is distributed in the cytoplasm via its association with the microtubule-associated protein Keap1. Upon ER stress, Nrf2 is phosphorylated and thus dissociates from Kelch-like ECH-associated protein 1 (Keap1), leading to the entry of Nrf2 into the nucleus (14). Remarkably, however, $Nrf2^{-/-}$ cells are sensitive to ER stress–induced apoptosis. Furthermore, there is growing evidence that Keap1-Nrf2 activation coupled with ER stress can alter the apoptosis outcome, although the effects vary from the stimulation to inhibition of apoptosis, depending on the cell type and the chemical properties and dose of the stimulus used to modulate Nrf2 (15).

Epidemiological studies have linked the consumption of fruits and vegetables to a reduced risk of cervical cancer, particularly the small fruits that are rich sources of pharmacologically active stilbenes (10). The Xinjiang Uygur Autonomous Region is an economically repressed area in China but is rich in natural resources, particularly grapes and berries. As constituents of small fruits, such as grapes and berries and their products, stilbenes are under intense investigation as cancer chemopreventive agents. In particular, the chemotherapeutical characteristics of pterostilbene (Pte), a stilbene found in blueberries and grapes, was demonstrated in previous studies. Experimental evidence shows that Pte has potential in the prevention or treatment of colon, liver, skin, pancreatic, lung, breast cancer, and leukemia (16). Various molecules and signaling pathways are involved in the anti-tumor effects of Pte, including cytosolic Ca^{2+} overload (17), adenosine monophosphate–activated protein kinase (AMPK) signaling (18), autophagy (19), ROS (19), Wnt signaling (20), Notch1 Signaling (21), and lysosomal membrane permeabilization (22). Regardless, there is no evidence thus far to indicate the pro-apoptotic effects of Pte on cervical cell lines. Thus, to better understand the chemotherapeutic effects of Pte, the present study aims to determine whether Pte induces apoptosis in the HeLa human cervical adenocarcinoma cell line by studying the involvement of the intrinsic apoptosis pathway and the role of cellular redox homeostasis in association with Pte treatment.

Materials and Methods

Chemical reagents

Fetal bovine serum (FBS) was purchased from Sijiqing (Hangzhou Sijiqing Co., Hangzhou, China). Pterostilbene (Pte), methyl thiazolyl tetrazolium (MTT), Hoechst 33258 and 33342, 2,7-dichlorodihydrofluorescein diacetate (H2DCFDA), L-*S*,*R*-buthionine sulfoximine (BSO), catalase (CAT), *N*-acetyl-L-cysteine (NAC), thapsigargin (TG), *tert*-butylhydroquinone (tBHQ), and dimethyl sulfoxide (DMSO) were purchased from Sigma Chemical Co. (St. Louis, MO, USA). 5-Chloromethylfluorescein diacetate (CMF-DA) was purchased from Molecular Probes (Eugene, OR, USA), and gentamicin was obtained from Shandong Sunrise Pharmaceutical Co., Ltd. (Zibo, China). All other chemicals were of analytical grade and were commercially available.

Cell culture and treatments

HeLa cells (ATCC Number: CCL-2) were purchased from ATCC (Manassas, VA, USA) and cultured in ATCC-formulated Eagle's Minimum Essential Medium with 10% FBS and 10 μg/mL gentamicin at 37°C in 5% CO_2. For all experiments, HeLa cells were seeded at 2×10^5 cells/mL. The cells were treated with Pte at the indicated concentration for 48 h either alone or in combination with a redox modulator for 4 h prior to Pte treatment. The concentrations used for the redox modulators are as follows: CAT (200 U/mL), NAC (200 μM), BSO (200 μM), TG (1.5 μM), and tBHQ (15 μM). These redox modulators except TG have been shown to have no significant effect on the basal levels of cell apoptotic markers at the indicated concentration and duration.

Cell viability assay

Cell viability was measured using the MTT assay (23). Cells were briefly trypsinized, seeded into 96-well plates at 4×10^3 cells/well, and pre-incubated for 24 h before treatment. The cells were then exposed to different concentrations of Pte, as indicated in Fig. 1a, at 37°C. The medium was removed after incubation, and fresh medium containing 10 μL of 5 mg/mL MTT was added; this medium was removed after 4 h and replaced with blue formazan crystal dissolved in 100 μL DMSO. The absorbance at 570 nm was measured using a microplate reader (Thermo Varioskan Flash 3001, USA). The cell inhibition rate was calculated as 100% × (control group A values − experimental group A values) / control group A values.

Determination of cell apoptosis

The morphological changes in the nuclear chromatin of cells undergoing apoptosis were detected by Hoechst-

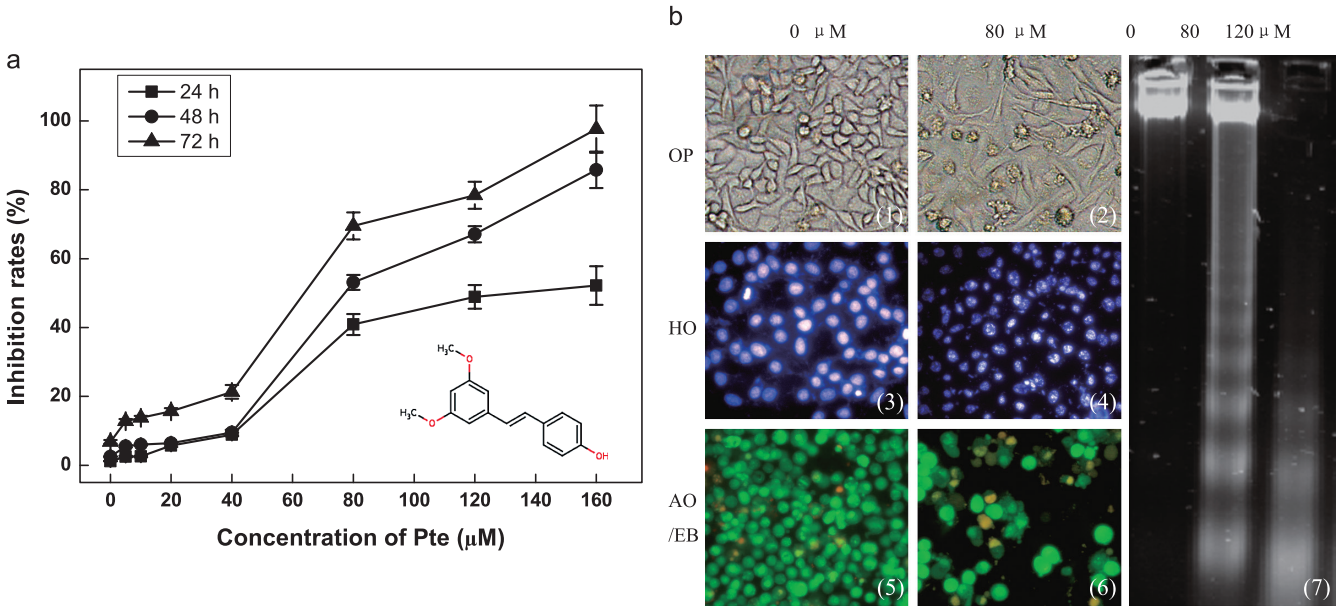

Fig. 1. Pte inhibits proliferation and induces apoptosis in HeLa cells. a): The effects of Pte on HeLa cell proliferation. The inhibition ratio of cell proliferation was determined by the MTT assay after 24-, 48-, and 72-h incubations with Pte at the indicated concentrations. All the data are presented as the mean ± S.E.M. of the results from three independent experiments; b): morphological characteristics and fragmentation of genomic DNA in Pte-treated HeLa cells (magnified 200 ×): (1), (3), (5): HeLa cells without Pte treatment. (2), (4), (6): HeLa cells treated with 80 μM Pte for 48 h; the images in (1) and (2) were captured using a light microscope to show the morphological changes of HeLa cells; the images in (3) and (4) were captured using a fluorescence microscope to show the morphological changes of HeLa cell nucleus; the images in (5) and (6) were captured using a fluorescence microscope in terms of AO/EB staining to show the differences in HeLa cell apoptosis and necrosis. (7): DNA ladder of HeLa cells observed after the exposure to Pte for 48 h. Left lane: control sample without Pte treatment. Middle lane: sample treated with 80 μM Pte. Right lane: sample treated with 120 μM Pte.

33258 and AO/EB staining. Briefly, HeLa cells treated with or without Pte were detached with trypsin-EDTA in DMEM, washed in PBS, and resuspended in 50 μL of 3% paraformaldehyde. The cells were then stained using either 8 μg/mL Hoechst-33258 stain or 100 μg/mL AO/EB stain in PBS. The apoptotic and necrotic cells were recorded by fluorescence microscopy (Axio Observer A1; Zeiss, Germany); a minimum of 400 cells were counted for each experiment for the apoptotic rate calculation according to the Hoechst-33258 stain results. For the DNA ladder assay, HeLa cells treated with or without Pte were collected by centrifugation at 1,000 × *g* for 5 min and washed with PBS. A 100-μL aliquot of lysis buffer (20 mM EDTA, 50 mM Tris-HCl, and 1% NP-40) was added to the pellets; 25 mg/mL proteinase K was added to the supernatant after centrifugation. After treatment with 10 M ammonium acetate and precipitation on ice, the samples were washed with 80% ice-cold ethanol and air-dried. The final pellet was dissolved in TE buffer, and DNA fragmentation was assayed by 2% agarose gel electrophoresis and imaged using a GelDOC system (Bio-Rad, Hercules, CA, USA).

Determination of intracellular ROS, GSH, and GSSG/GSH ratio

Cells were treated with the indicated chemical(s) for 4 h, washed with PBS, and treated with 20 μM H_2DCFDA (Ex/Em = 488 nm / 525 nm) or 5 μM CMFDA (Ex/Em = 492 nm / 517 nm) at 37°C for 30 min. The cells were washed twice with PBS, and the relative fluorescence intensity was measured by spectrophotometry. The ROS and GSH levels were calculated as the mean fluorescence intensity (MFI) per 1,000 non-necrotic cells, and the measurement of both probes in a single cell was performed using a fluorescence microscope. The cell numbers were calculated by staining with Hoechst-33342 and propidium-iodide (Pi) (24, 25). Standard curves were generated by a series of cell densities, ranging from 5×10^6 to 5×10^3, in 96-well plates. The cells were collected, sonicated, and mixed with either 1.15 μg/mL Hoechst-33342 or 20 μg/mL Pi dye at a 1:9 ratio and maintained at 37°C for 30 min; the DNA-associated Hoechst and Pi fluorescence was measured at 460 nm and 620 nm, respectively. Subtracting the necrotic cells (Pi-stained cells) from the total number of cells (Hoechst-stained cells) produced the number of non-necrotic cells

in each treatment. For the GSSG/GSH assay, Pte-treated cells were collected by centrifugation at 500 × *g* for 10 min and washed twice with PBS. The harvested cells were re-suspended in protein removal reagent and vortexed vigorously. The samples were frozen rapidly with liquid nitrogen (twice) and thawed at 37°C and then at 4°C for 5 min; the supernatant was collected by centrifugation at 10,000 × *g* for 10 min. The GSH /GSSG ratio was determined using a GSH and GSSG assay kit (Beyotime Institute of Biotechnology, Shanghai, China) according to the manufacturer's instructions.

Immunoblotting of key molecules and quantification of caspase activity in the ER stress–related intrinsic apoptosis pathway

The HeLa cells were harvested and lysed in Immuno Precipitation Assay buffer (Sangong Co., Shanghai, China) containing protease inhibitor and phosphatase inhibitor, and the total cell lysates were subjected to SDS-PAGE. The separated proteins were transferred to nitrocellulose membranes (Millipore Corp., Billerica, MA, USA), and the membranes were blocked with 5% skim milk. A conventional immunoblot was performed using several Abs; chemiluminescence was detected using an ECL kit (Sangong Co.) and the multiple GelDOC system (Bio-rad). Antibodies against the following were used: GAPDH, phospho-PKR-like ER kinase (PERK), eIF2α, GRP78, and CHOP (Santa Cruz Biotechnology, Santa Cruz, CA, USA); phospho–Nrf2 (Abcom Co., Hong Kong, China). The activities of caspase-3, caspase-9, and caspase-4 were assessed using Fluorometric Assay Kits according to the manufacturer's protocol (BioVision, Milpitas, CA, USA). The assay is based on the detection of the cleavage of the substrate DEVD-AFC (AFC: 7-amino-4-trifluoromethyl coumarin) by caspase-3, substrate LEVD-AFC by caspase-4, and substrate LEHD-AFC by caspase-9. The fluorescence of AFC from an apoptotic sample with the control allows the determination of caspase-3, -4, and -9 activities, which are converted from a blue emission (λ = 404 nm) to a yellow-green color (λ = 505 nm) (Thermo Varioskan Flash 3001; Thermo Fisher Scientific Inc., Waltham, MA, USA).

Evaluation of Nrf2/ARE and ER stress pathway–related gene expression

To analyze the expression levels of the ER stress–related genes GRP78 and CHOP (after 48 h of Pte treatment) and Nrf2 downstream target genes (after 4 h of Pte treatment), the cells were treated as indicated, washed with PBS, and collected. RNA was extracted from the cells using EZ-10 Spin Column Total RNA Minipreps Super Kit (Bio Basic, Inc., Markham, CA, USA) according to the manufacturer's instructions. The RNA quality was assessed using the A260/A280 ratio and 1.5% agarose gel electrophoresis. Two micrograms of RNA per sample was converted to cDNA using Moloney Murine Leukemia Virus reverse transcriptase with a First Strand cDNA Synthesis Kit according to the manufacturer's instructions (Fermentas, Vilnius, Lithuania). The cDNA was used for reverse transcription (RT)-PCR using ER stress– and Nrf2-related gene-specific primers according to previous studies (25, 26). The PCR primers (synthesized by Sangon Co.) and their cycling conditions are indicated in Table 1. The reaction conditions included 12.5 μL 2 × PCR Master Mix (Sangong Co.), 3 μL cDNA template, and 0.5 μL each primer. The semi quantitative RT-PCR products were assayed by 0.5% agarose gel electrophoresis using a GelDOC analysis system (Bio-rad).

Quantitative real-time RT-PCR was performed using

Table 1. Primer sequences table

Gene	Primers	Tm (°C)
GRP78	sense: 5′-TAGCGTATGGTGCTGCTGTC-3′ anti-sense: 5′-TTTGTCAGGGGTCTTTCACC-3′	58
CHOP	sense: 5′-AGCTGAGTCATTGCCTTTCT-3′ anti-sense: 3′-CTGGTTCTCCCTTGGTCTTC-5′	58
NQO1	sense: 5′-GAGGACCTCCTTCAACTATGCC-3′ anti-sense: 5′-CCTTTGTCATACATGGCAGCG-3′	59
GPX	sense: 5′-GGGGCCTGGTGGTGCTCGGCT-3′ anti-sense: 5′-CAATGGTCTGGAAGCGGCGGC-3′	65
CAT	sense: 5′-AACTGGGATCTTGTGGGAA-3′ anti-sense: 5′-GACAGTTCACAGGTATCTG-3′	55
GR	sense: 5′-GAAAAGGCTGTAATTTTATTTTCAA-3′ anti-sense: 5′-ATCAAAAGTCCCTTCCTCTGC-3′	55
GAPDH	sense: 5′-CAAGGTCATCCATGACA-ACTTTG-3′ anti-sense: 5′-GTCCACCACCCTGTTGCTGTAG-3′	57

a single-tube SYBR Green kit (QIAGEN, Valencia, CA, USA), Rotor Gene Q real-time PCR system (Rotor Gene Q, QIAGEN), and specific primer sets (the same primers used in the conventional RT-PCR). Only experiments in which a distinct single peak was observed, with a melting temperature different from that of the no-template control, were analyzed. The relative amount of target mRNA was calculated by the $2^{-\Delta\Delta Ct}$ method. Each sample was analyzed using glyceraldehyde-3-phosphate dehydrogenase (GAPDH) as an endogenous reference gene for mRNA normalization.

Statistical analyses

The data obtained from different experiments are presented as the mean ± S.D. of at least three independent experiments and were evaluated by ANOVA. Student's *t*-test for multiple comparisons was used to identify differences among the groups. The values were considered to be statistically significant at $P < 0.05$.

Results

Pte inhibits the proliferation of HeLa cells

Previous studies have determined that the optimal cytotoxic dose range of Pte ranges from 2.96 to 93.4 μM (16). Therefore, the experiments in the present study employed a concentration range of 5 to 160 μM Pte to study its inhibition on HeLa proliferation after various times. According to the MTT assay, HeLa cell proliferation was inhibited in a dose-dependent manner compared to that of the control group (0 μM). The inhibition rates showed a significant "S" shape curve (Fig. 1a), with a rapid increase in the inhibition rate in all time-interval groups as the concentration of Pte increased from 40 to 80 μM. At 80 μM, Pte had an inhibition rate of 53.1% after 48 h, which was almost equivalent to the IC_{50} value. The Pte inhibitory rate on HeLa cell was the highest at 160 μM after a 72-h treatment. These results indicated that the inhibitory potency of Pte on HeLa cell proliferation was related to the duration of the treatment. Therefore, we selected a relatively higher concentration range from 80 to 120 μM and a 48-h time interval for the investigations involving in the cytotoxic effects of Pte on HeLa cells.

The pro-apoptotic effects of Pte on HeLa cells

Cells grown under the influence of Pte quickly exhibited morphological changes in the cell membrane and nucleus that were characteristic of apoptosis. As shown in Fig. 1b, in comparison to the control cells, the Pte-treated HeLa cells were shrunken and showed the typical membrane blebbing. Further apoptotic evidence was indirectly shown with fluorescent dyes. The Hoechst-stained untreated control cells displayed rounded nuclei containing diffuse Hoechst-stained chromatin. After Pte treatment, the cell nuclei became granular, which indicates nuclear fragmentation as a typical apoptotic effect. To confirm the pro-apoptotic effect of Pte, the Pte-treated cells were evaluated using the DNA ladder assay. Treatments of both 80 and 120 μM Pte resulted in significant DNA fragmentation that was stronger in the latter. Because necrotic effects were possible, the cells were stained with AO/EB to further demonstrate the killing effect of Pte. Normal viable HeLa cells were stained green, without membrane bubbles (control), whereas the apoptotic HeLa cells with Pte treatment appeared as bright green arcs in the early stage and with condensed, yellow/orange nuclei in the late stage, but no necrotic cells were observed (Fig. 1b).

The intracellular redox homeostasis shifts toward oxidation with Pte-induced HeLa cell apoptosis

The fluorescent probes H_2DCFDA and CMF-DA were used to evaluate the level of the intracellular redox products ROS and GSH in HeLa cells (Fig. 2a). The duration of HeLa cell exposure to Pte was limited to 4 h, the time frame in which ROS events are initiated prior to drug-induced apoptosis, as described in previous works (25). The relative DCF fluorescence density (mean ROS production) significantly increased with 0 – 160 μM Pte treatment, whereas the relative CMF fluorescence density (mean GSH production) increased with 0 – 80 μM Pte treatment and decreased inversely from 80 to 160 μM Pte. To define the precise changes in the intracellular redox homeostasis, the ratio of total GSH to its oxidized product (GSSG) was analyzed after Pte treatment. The results showed that treatment with Pte consistently reduced the GSH/GSSG ratio, indicating an intracellular redox homeostasis shift toward oxidation (Fig. 2b).

The involvement of ER stress in Pte-induced HeLa cell apoptosis

The intrinsic pathway is mainly involved in redox-modulated drug-induced cell apoptosis due to intracellular thiols coupled with mitochondrial and ER stress. Therefore, the key molecules caspase-3, -4, and -9 were assayed in the present study, with a significant increase after exposure to 80 μM Pte for 48 h (Fig. 3a). Within the context of activated caspase-3 and -4 in the ER apoptotic pathway, Pte treatment was found to up-regulate the effects of ER stress signals on the α-subunit of eIF2α and PERK phosphorylation, involving the accumulations of 78-kDa glucose-regulated protein (GRP78) and C/EBP homologous protein (CHOP) (Fig. 3b). Stronger evidences were revealed through

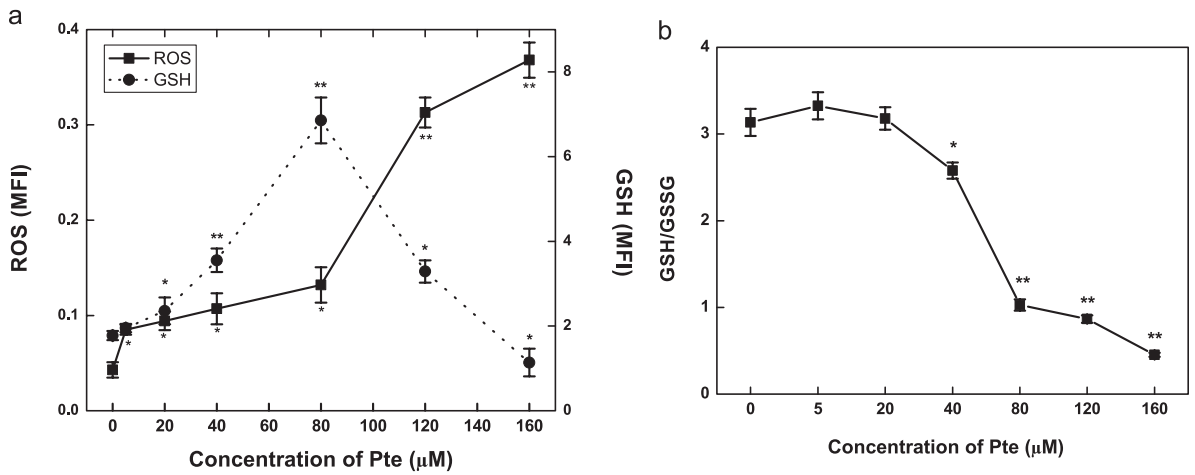

Fig. 2. The changes in the intracellular redox homeostasis in HeLa cells prior to Pte-induced apoptosis. a) The changes in the intracellular ROS and GSH levels in HeLa cells treated with Pte at the indicated concentrations for 4 h. The ROS and GSH levels were calculated as the mean fluorescence intensity (MFI) per 1,000 non-necrotic cells. b) The changes in the intracellular GSH/GSSG ratios in HeLa cells treated with Pte at the indicated concentrations for 4 h. All the data are presented as the mean ± S.E.M. of the results from three independent experiments. *$P < 0.05$, **$P < 0.01$, compared to the Blk (Control) group.

additional experimental semi/full-quantitative assays of markers in the ER stress pathway. The expression of GRP78 and CHOP were markedly increased after 48 h treatment with 80 and 120 μM Pte, with the latter group showing the higher level (Fig. 3: c and d).

The intracellular redox homeostasis is closely associated with Pte-induced HeLa cell apoptosis

To understand whether the observed changes in intracellular redox homeostasis were important determinants of Pte-induced cell apoptosis, it was necessary to correlate the level of produced ROS and/or GSH to the extent of the event. The addition of the pro-oxidant BSO and a ER-stress inducer TG, as described in the methods, significantly enhanced ROS by reducing GSH in the Pte-treated cells (Fig. 4a). Pte-induced cell apoptosis was further facilitated with the enhanced activities of caspase-3 and -4 and the increased mRNA expression levels of GRP78 and CHOP (Fig. 4: b, c, d, and e).

In this study, both enzymatic and non-enzymatic anti-oxidative agents were used to identify the key redox events involved in Pte-induced apoptosis. When the GSH precursor NAC and Nrf2 activator tBHQ were added, GSH production was increased and was concurrent with the alleviated ROS production (Fig. 4a). In contrast to the BSO co-treatment, both anti-oxidants significantly suppressed Pte-induced cell apoptosis, with reducing the activities of caspase-3, -4 and decreasing the mRNA expression levels of GRP78 and CHOP (Fig. 4: b, c, d, and e). After the enzymatic anti-oxidative enzyme CAT, which functions as an H_2O_2 scavenger, was added prior to Pte treatment, a similar trend was observed in the suppression of ROS production and also in the restoration of GSH (Fig. 4a). The kinetics of caspase activity and the mRNA expression levels of GRP78 and CHOP in HeLa cells in the presence of CAT are shown in Fig. 4, b, c, and d. The addition of CAT suppressed the Pte-induced apoptosis in HeLa cells (Fig. 4e) and also demonstrated a strong inhibition of the expression of GRP78 and CHOP mRNA.

Redox homeostasis-mediated Nrf2 and ER stress are involved in Pte-treatment

It has been previously demonstrated that Nrf2 is activated following pharmacologically induced ER stress via PERK-mediated phosphorylation (27). To determine whether Nrf2 participates in the pharmacological response to Pte-induced ER stress through PERK-dependent regulation, the phosphorylation of PERK and Nrf2 were examined in Pte-induced HeLa cell apoptosis. As shown in Figs. 3b and 5, ER stress activation was shown by the forced expression of GRP78 and CHOP in a dose dependent manner within Pte treatments, which resulted in the enhanced Nrf2 phosphorylation. As previously described, the redox modulators alter the status of the unfolded protein response (UPR), coupled with the expression of GRP78, CHOP, and the phosphorylations of PERK and Nrf2. BSO and TG enhanced Pte-induced ER stress and Nrf2 phosphorylation levels. In contrast, both CAT and NAC reduced the Pte-induced ER stress, resulting in decreased PERK and Nrf2 phosphorylation levels, in accordance with the changes in the

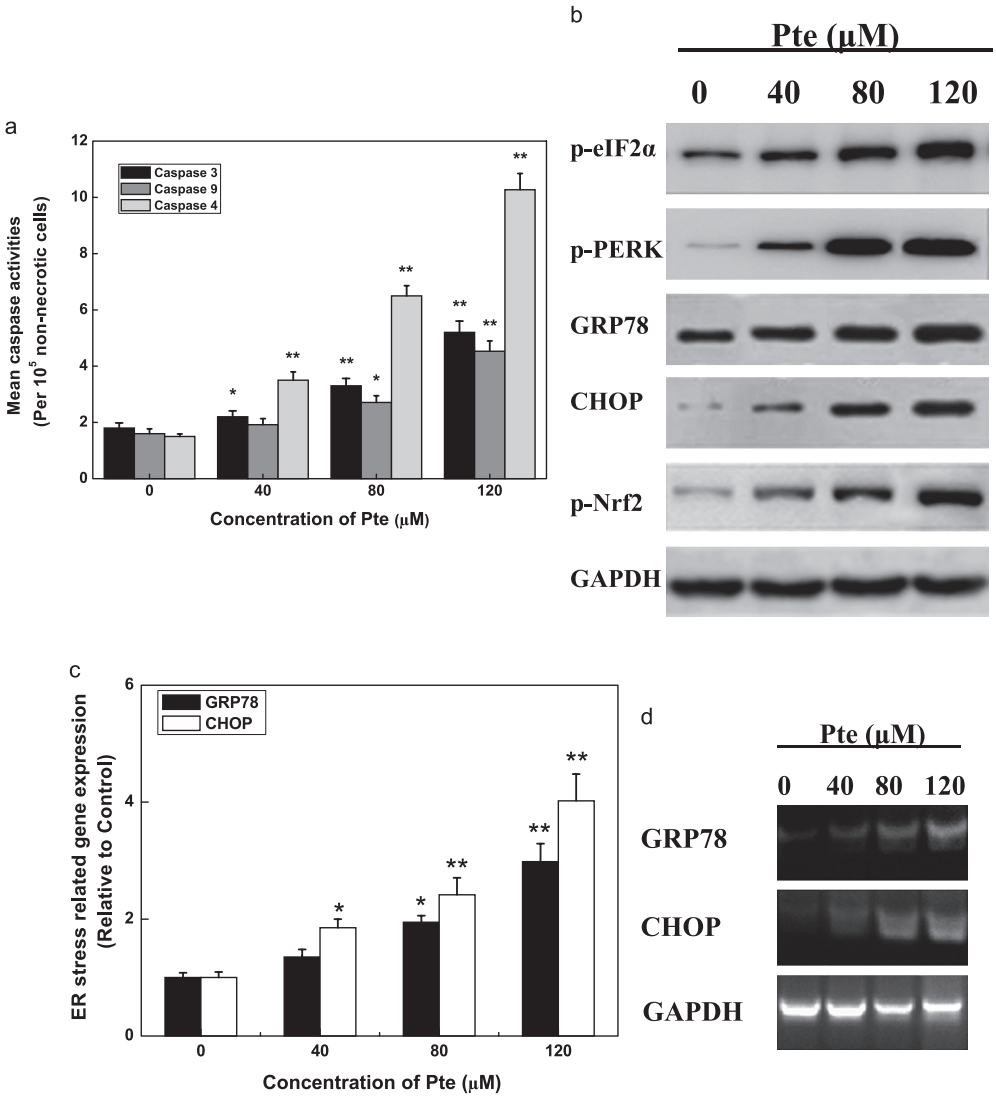

Fig. 3. The involvement of the endoplasmic reticulum pathway in Pte-induced HeLa cell apoptosis. a) The activities of caspase-3, -4, and -9 of the intrinsic apoptosis pathway in Pte-induced HeLa cell apoptosis after 48-h treatments. Data were calculated as the mean fluorescence intensity (MFI) per 100,000 non-necrotic cells. b) Immunoblotting of key molecular markers from ER to Nrf2 pathway after Pte treatment for 48 h. c) The expression level of key molecules monitored by real-time PCR analyses and normalized to the levels of GAPDH in the ER stress pathway after 48-h Pte treatments. d) Those expression levels were monitored by semi-quantitative RT-PCR assay. All the data are presented as the mean ± S.E.M. of the results from three independent experiments. $*P < 0.05$, $**P < 0.01$, mean compared to the Blk group; $^{\#}P < 0.05$, $^{\#\#}P < 0.01$, mean compared to Pte group.

expression of GRP78 and CHOP (Figs. 4 and 5). tBHQ reduced the Pte-induced ER stress but activaed P-Nrf2 (Fig. 4: c, d and Fig. 5).

The Nrf-2/ARE signaling pathway is involved in the response to Pte treatment

The ARE-regulated gene expression levels representing intracellular redox homeostasis can be used to determine whether the pro-apoptotic effect of Pte is associated with its ability to activate the Nrf2/ARE pathway as a direct result of active Nrf2 in HeLa cells. The major Nrf2/ARE-regulated gene products, NADP(H):quinine oxidoreductase-1 (NQO1), glutathione peroxidase (GPX), glutathione reductase (GR), and CAT (25, 28), were analyzed in terms of their mRNA expression levels. As shown in Fig. 6, a, b, and c, the mRNA expression levels of NQO1, GPX, and CAT were markedly up-regulated by Pte in a dose-dependent manner; in contrast, the gene expression level of GR was suppressed with increasing Pte concentration.

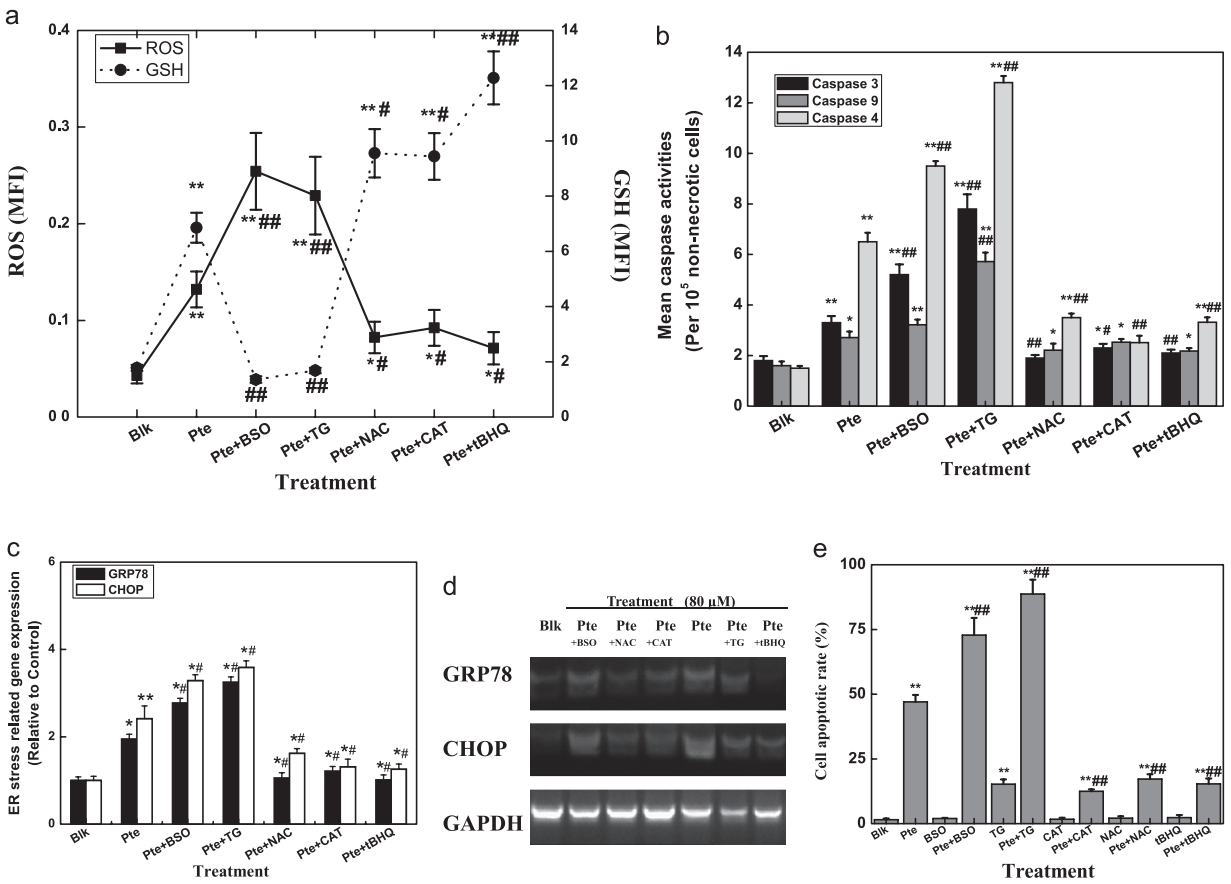

Fig. 4. Effects of redox modulators on Pte-induced HeLa cell apoptosis. a) The changes in the intracellular ROS and GSH levels in HeLa cells treated with BSO, TG, CAT, NAC, and tBHQ prior to 80-μM Pte treatment for 4 h. b) The changes in the activities of caspase-3, -4, and -9 by BSO, TG, CAT, NAC and tBHQ pretreatments prior to 80-μM Pte treatment; c) The expression level of key molecules in the ER stress pathway after BSO, TG, CAT, NAC, and tBHQ pretreatments and 48-h Pte (80 μM) treatments. The transcript levels were monitored by real-time PCR analyses and normalized to the levels of GAPDH. d) Those expression levels were monitored by semi-quantitative RT-PCR assay. e) The effects of redox modulators on 80 μM Pte–induced HeLa cell apoptotic rates. All the data are presented as the mean ± S.E.M. of the results from three independent experiments. $^{*}P < 0.05$, $^{**}P < 0.01$, compared to the Blk group; $^{\#}P < 0.05$, $^{\#\#}P < 0.01$, compared to the Pte group.

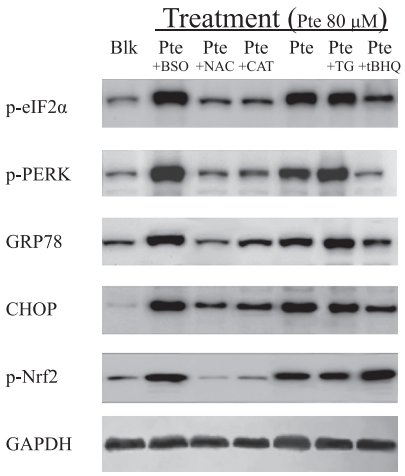

Fig. 5. The changes of key molecules from ER to the Nrf2 pathway in response to redox modulator pretreatment (4 h) and 80-μM Pte treatment (48 h).

Based on these observations, we can better understand the kinetics of the Nrf2/ARE signaling pathway in response to Pte treatment in HeLa cells. However, the enhancement or suppression of cell apoptosis mediated by the redox modulators from the Nrf2/ARE signaling pathway requires further detailed explanation. As shown in Fig. 6, d, e, and f, BSO pretreatment facilitated cell apoptosis and showed the highest NQO1 expression level and the lowest GR expression level with all the Pte treatments. The level of NQO1 expression was decreased in the other treatments found to inhibit Pte-induced cell apoptosis, whereas GR expression was increased. Interestingly, both enzymatic and non-enzymatic agents reduced the CAT gene expression level more efficiently compared to the Pte treatment alone (Fig. 6b).

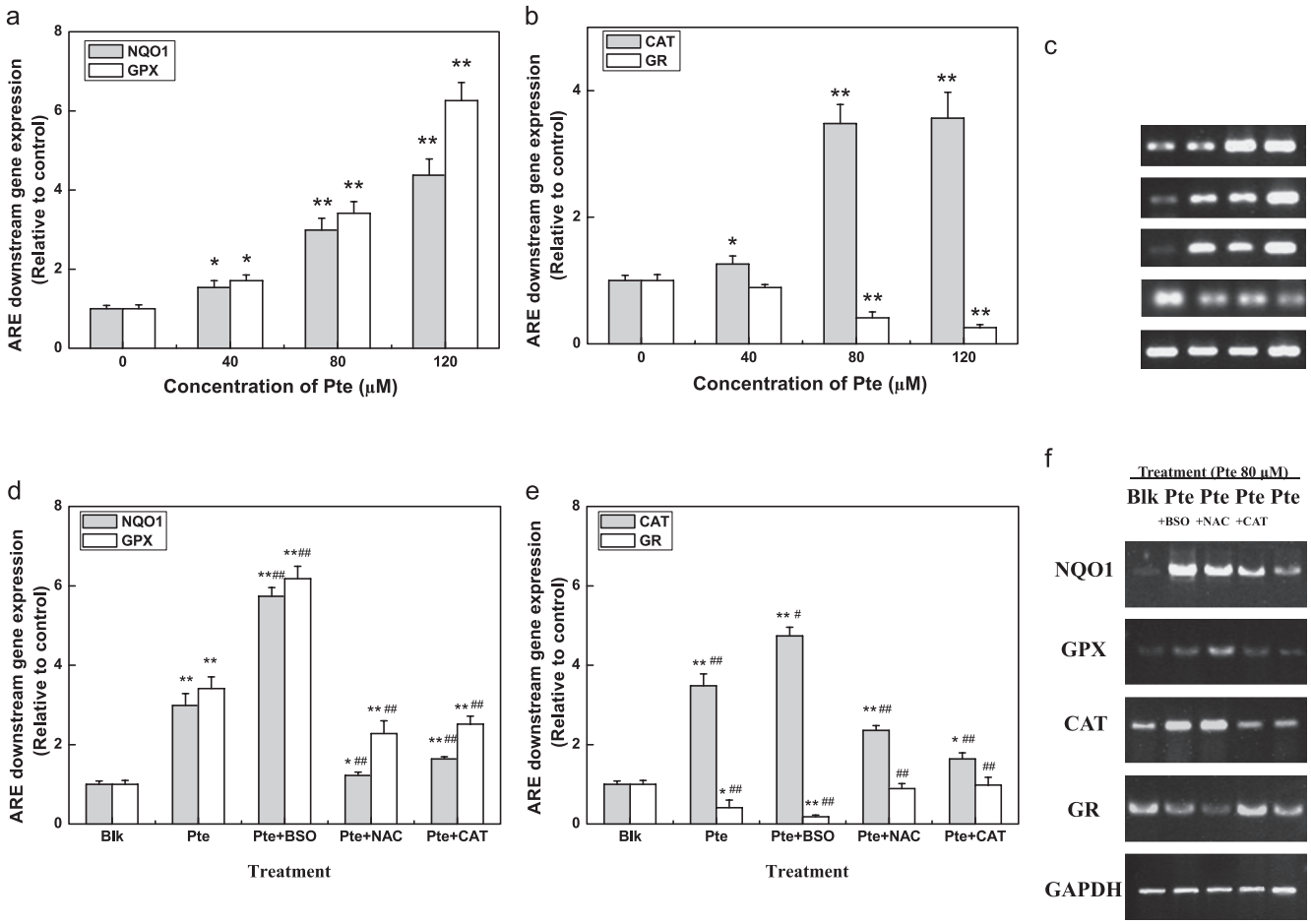

Fig. 6. The modulation of the downstream target genes of the Nrf2/ARE pathway in Pte-induced HeLa cell apoptosis. The mRNA expression levels of the GPX, GR, NQO1, and CAT genes in HeLa cells after 4 h of treatment with Pte at the indicated concentrations, a) Realtime PCR assay for NQO1 and GPX genes; b) Realtime PCR assay for CAT and GR genes; c) semi-quantitative RT-PCR assay for those ARE downstream target genes, the mRNA expression levels of the GPX, GR, NQO1, and CAT genes in HeLa cells after 4-h pretreatments with BSO, CAT, and NAC and then treatment with 80 μM Pte for 4 h; d) realtime PCR assay for NQO1 and GPX genes; e) realtime PCR assay for CAT and GR genes; f) semi-quantitative RT-PCR assay for those ARE downstream target genes; all the data are presented as the mean ± S.E.M. of the results from three independent experiments. *$P < 0.05$, **$P < 0.01$, compared to the Blk group; $^{\#}P < 0.05$, $^{\#\#}P < 0.01$, compared to the Pte group.

Discussion

Grape and blueberries are popular small fruits worldwide. In an previous effort to identify the chemopreventive effects on cancer cells of ethanol extracts from certain edible berries, strawberry and blueberry extracts were found to significantly decrease the growth of cervical and breast cancer cells, with blueberry extracts inhibiting the growth of the cervical cancer cells more than that of the breast cancer cells (10, 29). Pte, a resveratrol analog, was originally found by Langcake and Pryce to be a major component of the ethanol extracts of those fruits, and its pharmacological activities, including anti-oxidant activity and antibacterial, anti-inflammatory, and anti-tumor effects, have been characterized (30). Previous in vitro studies showed the cellular growth inhibition by Pte on various tumor cell lines with different sensitivities and conditions (16, 31). For example, in leukemia cells, antiproliferative activities were shown with IC_{50} values of 35 μM (HL-60), 42 μM (HL-60R), and 10 μM (K562). In colon carcinoma cells, inhibition of cancer cell viabilities were shown with IC_{50} values of 23.8 μM (HT29), 2.9 μM (26-L5), and 14.46 μM (Caco-2). Other literature has confirmed the different toxicities of Pte on cancer cells, with IC_{50} values of 71.7 μM (A549), 93.4 μM (HT1080), 15.9 μM (B16-BL6), 10 μM (MDA-MB-231), and 9.43 μM (HeLa) (Supplementary Fig. 1: available in the online version only and Table 1).

The present study found that the IC_{50} value of Pte on

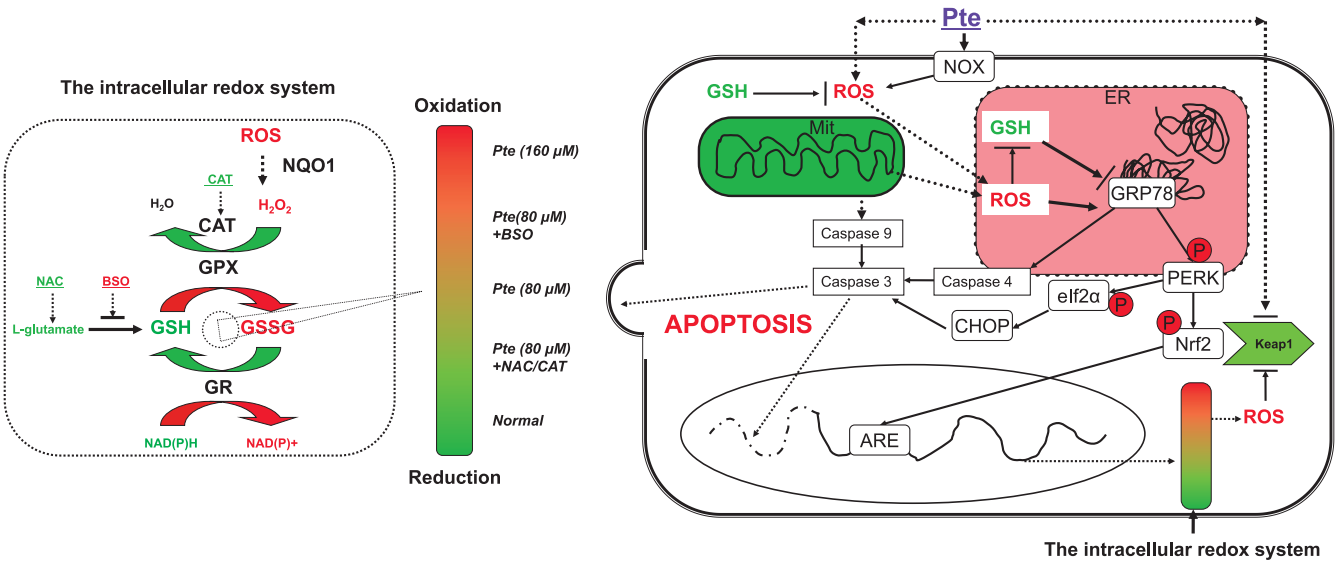

Fig. 7. Schematic representation of the role of redox homeostasis in Pte-induced HeLa cell apoptosis. Pte trigged ER-stress by redox imbalance, which was negatively regulated by a following activation of Nrf2.

HeLa cells was approximately 60 μM at 72 h, at the midpoint considering a PUBCHEM report (IC_{50} from 2.96 to 93.4 μM) (16), and the IC_{50} value in the present study was quite different from that in a previous report, 9.43 μM at 72 h (32). Although there were differences in the purity of Pte, and also in the methodology/conditions used, the chemical toxic sensitivities were similar. According to a NCI record (Compound 327430) (http://dtp.nci.nih.gov) and a PUBCHEM record (Compound 445154) (http://pubchem.ncbi.nlm.nih.gov), breast, colon, and cervical cell lines that are sensitive to Pte are also sensitive to resveratrol treatments in vitro (16, 31) (Supplementary Table 1: available in the online version only). We had evaluated the specificity of Pte against different diseases according to inferred scores in the Comparative Toxicogenomics Database (CTD) (33). The inferred relationships had been established between Pte and diseases. Among the top 100 inferred diseases, evidences suggested that cancer (Supplementary Fig. 1c) and cardiovascular disease (data not shown) are highly correlated with Pte. Pathways analysis had also been retrieved from CTD and enriched significantly among genes that interact with Pte (data not shown). Genes involved into the pathways in cancer (ranking 1st) and apoptosis (ranking 7th) were highly annotated in Pte treatments. Those evidences pointed out the possible pro-apoptotic activity of Pte for potential application in treating cancer disease. Additionally, the cytotoxicity data in vitro of Pte and 10 analogues were retrieved from the PUBCHEM database to display the specificities and structure–activity relationships on cancer cell lines (Supplementary Fig. 1: a and b). It is clear that Pte is specific to colonic neoplasms (26-L5, Caco-2), adenocarcinoma (HeLa), and breast neoplasms (MCF-7, MDA-MB-231) according to CTD and PUBCHEM records (Supplementary Fig. 1: c, d and Table 1). Among all analogues, beta-asarone (IC_{50} = 126.11 μM), resveratrol (IC_{50} = 58.86 μM), pinostilbene (IC_{50} = 48.4 μM), together with Pte (IC_{50} = 9.43 μM) had shown a tendency toward lower IC_{50} on HeLa cells. Thus it was suggested that the cytotoxicity of Pte and its analogues depends significantly on the structural determinants, which are double bond and methylated phenolic hydroxyl (Supplementary Fig. 1: a and e) (34). Therefore Pte can serve as a lead compound to derive other analogues with higher therapeutic efficacy.

Pte is not known to be toxic or cause adverse effects in humans. In mice fed Pte for 28 days at doses up to 3000 mg/kg body weight/day, equivalent to 500 times the estimated mean human intake (25 mg/day), no significant toxic effects or adverse biochemical parameters were noted, compared to controls (35). Recent reports suggest that in humans Pte up to a dose of 250 mg/day does not have any adverse toxic effects on hepatic and renal functions, thereby emphasizing its importance as a safe drug (36).

The antiproliferative activity of Pte in terms of cell differentiation, apoptosis, and/or necrosis was observed within the reported concentrations (16). Among the cytotoxic events, pro-apoptotic effects were observed in the present work. Lower cytotoxicity and higher protective potency seemed to be common characteristics

of natural stilbenes. However, early efforts were made to assess their anticarcinogenic activity in vivo and in vitro, which showed quite large differences. In leukemia cells, it was found that Pte (IC_{50} = 35 μM) was less toxic than resveratrol (IC_{50} = 5 μM) (37). Similarly, compared to our previous report in inducing apoptosis in HeLa cells, Pte was used at a higher concentration (IC_{50} = 80 μM) than resveratrol (IC_{50} = 40 μM) (38). Interestingly, resveratrol given orally had no effect on leukemia and lung cancer (39, 40). Nevertheless, injected intraperitoneally, 2.5 or 10 mg/kg of resveratrol slowed the growth of metastatic Lewis lung carcinomas in mice (40, 41). Due to the low aqueous solubility and fast metabolism of resveratrol in the human body, stilbene's potential value against cancer which was based at higher concentration in vitro, however, only existed in cancer prevention in vivo. Since substitution of a hydroxy group by a methoxy group increases the transport into cells and increases the metabolic stability of Pte (Fig. 1a), it show higher biological activity based on relatively higher bioavailability compared to resveratrol (42). Different published data in vitro show that Pte has a potent activity with lower toxicity in various cancer types at concentration ranges from 0 to 100 μM (A375, A549, HT29, MCF7, NCI-H460, SK-MES-1) (22, 43, 44). Further, it was found in human colon cancer cells that the higher intracellular levels of Pte than resveratrol may be associated with higher lipophilicity of Pte in comparison with resveratrol (44). Taken together, higher concentration of Pte in the present study indicated that it has less toxicity but possesses a pro-apoptotic activity that warrants its consideration for future in vivo research.

The unique ROS metabolism in cancer cells may represent a therapeutic target (10, 11). Indeed, the variety of ROS levels after Pte treatment was a primary focus in the present study. We observed a rapid enhancement in ROS production (Pte from 0 to 160 μM) and GSH depletion (Pte from 80 to 160 μM) as a preliminary effect of Pte-induced HeLa cell apoptosis, in agreement with previously published pro-apoptotic reports in other cell lines (21, 45,46). Stilbenes, including Pte, have also been reported to generate ROS and electrophilic molecules (19, 21, 47). Nevertheless, other research has revealed that Pte shows highly efficient anti-oxidative activities against several types of ROS (48). Within this context, a simple explanation for Pte-induced apoptosis was difficult to provide with regard to the production of ROS alone. The three most important redox systems within the cells are NADPH/$NADP^+$, thioredoxin (TRXred/TRXox), and glutathione (GSH/GSSG). Among these systems, GSH/GSSG is the most important because glutathione concentrations are approximately 500 – 1000-fold higher than NADPH and TRX; thus, changes in reduced oxidized glutathione directly reflect intracellular redox alterations coupled to various cell processes (12). Redox homeostasis is thought to play an important role in HeLa apoptosis (15, 49), and the redox homeostasis of GSH/GSSG in the Pte-treated cells was shifted toward oxidation in a dose-dependent manner, suggesting higher levels of oxidative stress prior to the induced apoptosis (21). Further, in Fig. 2a, the increased ROS by Pte from 80 to 160 μM caused a depletion of GSH in the total glutathione pool (Fig. 2b), while the increasing of GSH with additional Pte (0 to 80 μM) could not be well understood without considering the dynamic compensation in the total glutathione pool by activated Nrf2 pathway gene products which will be discussed in the following paragraphs (50).

The exact mechanisms that regulate apoptosis through the ER are not well understood. Several different pathways have been implicated, including the caspase-12/caspase-4 pathway. The role of caspase-12 in ER-mediated apoptosis is well established in mice (51). However, its role in apoptosis of human cells is unresolved, since the human caspase-12 gene contains several inactivating mutations (52). Caspase-4 is the best candidate that would function similarly to mouse caspase-12 in ER stress–induced cell death in humans (53, 54). Our results, based on enzymatic assay, show the relative levels of apoptotic signals in classic caspase 3, 4, and 9. Redox imbalance caused by either experimental agents or pathophysiological conditions leads to the accumulation of unfolded/misfolded proteins in the ER lumen (12). Although the ER luminal and cytosolic glutathione concentrations are similar (i.e., 1 – 10 mM), the ratio of (GSSG) to (GSH) is higher in the ER compared to the cytosol. Thus, it is reasonable that the ER lumen is more sensitive in response to either pro-oxidants and/or their secondarily produced ROS. As has been described, stilbenes exhibit controversial anti-oxidative and pro-oxidative capabilities in vitro and in vivo. However, evidence from the intracellular redox imbalance caused by stilbenes supports the critical role in ER stress involved in the decision of cell fate. For example, the well-known anti-oxidant resveratrol actually triggers ER stress and dopaminergic cell death, and further involvement of ER stress in the induction of apoptosis by resveratrol was also proven in HT29 colon carcinoma cells (55). The ER-stress inducer TG showed a synergistic effect with Pte-treatment on the ROS production and apoptosis, suggesting the pro-oxidative role of Pte in HeLa cell apoptosis via ER stress.

Additional evidence was needed to determine the decisive role of redox homeostasis in cell death via the activity of both enzymatic and non-enzymatic anti-oxidants and/or pro-oxidants in Pte treatment. HeLa

cell apoptosis was enhanced with the specific depletion of GSH when co-treated with BSO, a selective and irreversible inhibitor of glutamate cysteine ligase (GCL), which coordinates GSH synthetase to synthesize GSH in the cytoplasm (56). However, HeLa cell apoptosis was suppressed with enhanced GSH production when co-treated with the GSH precursor NAC and peroxide scavenger CAT. All of the specific modulators of ROS and GSH were sufficient to interrupt redox homeostasis in the Pte-treated HeLa cells. Although the direct production of ROS by Pte or the involvement of ROS release from NADPH oxidase (NOX) and mitochondria (Mit) in HeLa cells cannot be ruled out, the data presented here suggest a mechanism for Pte-induced apoptosis: enhanced ROS production in addition to GSH depletion by Pte-induced oxidative stress in the HeLa cells, which resulted in the fine modulation of the intracellular redox homeostasis to facilitate apoptosis (21, 49, 57, 58). In the present study, the Pte-treated HeLa cells showed an induced ER overload response and ER stress, eliciting apoptosis through intracellular redox disorder, caspases activation, and GRP78 and CHOP expression. The further addition of CAT and NAC in the Pte treatments alleviated the Pte-induced apoptosis, with decreased expression of ER stress markers. All of these results suggest that the ER stress can be attributed to Pte-enhanced ROS production via a specific mechanism [i.e., Mit and/or NOX, as described previously (17, 21, 45, 59)] and also highlight the alteration of the defensive anti-oxidant response (14, 15).

When cells encounter oxidative stress, the Nrf2–ARE-mediated defensive cellular response is activated to remove and counteract the harmful effects of oxidative and xenobiotic agents. In a recent review, small molecule modulators of non-carcinogenic ARE inducers were listed as a chemoprevention strategy (60), with resveratrol being described as a potential ARE inducer. It is predictable that Pte as a resveratrol analog activates the Nrf2 pathway and causes alterations in ARE gene expression to disrupt the Halliwell–Asada pathway (61, 62). The well-known Nrf2 activator tBHQ displayed inhibitions on both ER stress and cell apoptosis in Pte treatments, suggesting the important role of the Nrf2 pathway in the regulation of Pte-induced apoptosis. The activation of the Nrf2 pathway resulted in the transcription of ARE downstream genes (NQO1, GPX, CAT, GR et al.). So mRNA assay by RT-PCR is necessary to verify the involvement of the Nrf2 pathway in Pte-treatment. GR is a key enzyme performing GSH synthesis in the Halliwell-Asada pathway, although GPX is responsible for GSH oxidation to GSSG by H_2O_2 (63). Pte suppressed the gene expression levels of GR but enhanced GPX in agreement with Chakraborty et al. (57), which is suggested to be responsible for the GSH depletion in the present study. The primary metabolic function of NQO1 is the reduction of quinones to hydroquinones, with the consumption of a reducing equivalent (NADPH). The inherent O_2^- scavenging activity of NQO1 is attractive because it could play a potential role in minimizing the deleterious consequences of the generation of redox-active hydroquinones, which also raises the issue of the relevance of this effect in cells in which there are more efficient systems for superoxide removal such as SOD (64). We observed a Pte-induced increase in the NQO1 expression level, which was markedly restored by co-treatment with all of the tested anti-oxidants, except for BSO, suggesting that the production of hydroquinones and glutathione-S-conjugates was increased. When coupled with the oxidative stress induced by Pte treatment, these findings emphasize the sensitivity of CAT in response to H_2O_2 detoxification. Both enzymatic and non-enzymatic anti-oxidative agents reduced the levels of NQO1, CAT, and GPX gene expression more efficiently compared to the Pte treatment alone. Furthermore, treatment with BSO caused GSH depletion in addition to the highest expression levels of the GPX gene. This evidence suggests that both enzymes play an important role in response to Pte-induced oxidative stress, coupled with GSH depletion and H_2O_2 production. Altogether, as shown in Fig. 7, evidence supported that Pte trigged ER-stress by redox imbalance which was negatively regulated by a following activation of Nrf2. These changes in the major Nrf2/ARE-regulated genes displayed a unique mechanism of anti-oxidative buffers and also triggered ER stress and resulted in Pte-induced HeLa apoptosis.

Collectively, our study is the first investigation of the pro-apoptotic effect of Pte on HeLa cells, specifically addressing the role of redox homeostasis in regulating HeLa cell apoptosis through the unique modulation of the ER/Nrf2 pathway. Further studies are needed to show the comparative chemotherapeutic potency of Pte on different cervical cancer cell lines and the post-translational modifications and enzymatic activities of the gene products in the Nrf2 pathway.

Acknowledgments

This Study was supported by the National Natural Science Foundation of China (No. 31160058), the key technology program (2014BA029), and the doctoral funds (No. 2011BB018) of Xinjiang Production & Construction Corps.

Conflicts of Interest

The authors declare that they have no competing interests.

References

1 World Health Organization. Fact sheet No. 297. Cancer. 2013.
2 Kent A. HPV Vaccination and testing. Rev Obstet Gynecol. 2010;3:33–34.
3 Ferlay J, Bray F, Pisani P, Parkin DM. GLOBOCAN 2002. Cancer incidence, mortality and prevalence worldwide. IARC Cancer Base No. 5 Version 2.0. Lyon: IARC Press; 2004.
4 Sankaranarayanan R, Budukh AM, Rajkumar R. Effective screening programmes for cervical cancer in low- and middle-income developing countries. Bull World Health Organ. 2001; 79:954–962.
5 Vijaykumar DK. Chemotherapy for cervical cancer. Indian Journal of Medial and Paediatric oncology. 2008;29:6.
6 Surh YJ. Cancer chemoprevention with dietary phytochemicals. Nat Rev Cancer. 2003;3:768–780.
7 Sporn MB, Liby KT. Cancer chemoprevention: scientific promise, clinical uncertainty. Nat Clin Pract Oncol. 2005;2:518–525.
8 Marc JK, Michael SJJ, Ronald DA. Concurrent chemotherapy and radiation for advanced cervical cancer. CME Journal of Gynecologic Oncology. 2001;19:92–98.
9 Verreault R, Chu J, Mandelson M, Shy K. A case-control study of diet and invasive cervical cancer. Int J Cancer. 1989;43:1050–1054.
10 Wedge DE, Meepagala KM, Magee JB, Smith SH, Huang G, Larcom LL. Anticarcinogenic activity of strawberry, blueberry, and raspberry extracts to breast and cervical cancer cells. J Med Food. 2001;4:49–51.
11 Srinivas P, Gopinath G, Banerji A, Dinakar A, Srinivas G. Plumbagin induces reactive oxygen species, which mediate apoptosis in human cervical cancer cells. Mol Carcinog. 2004;40:201–211.
12 Schafer FQ, Buettner GR. Redox environment of the cell as viewed through the redox state of the glutathione disulfide/glutathione couple. Free Radical Bio Med. 2001;30:1191–1212.
13 Hayes JD, McMahon M. Molecular basis for the contribution of the antioxidant responsive element to cancer chemoprevention. Cancer Lett. 2001;174:103–113.
14 Cullinan SB and Diehl JA. PERK-dependent activation of Nrf2 contributes to redox homeostasis and cell survival following endoplasmic reticulum stress. Biol Chem. 2004;279:20108–20117.
15 Kensler TW, Wakabayashi N, Biswal S. Cell survival responses to environmental stresses via the Keap1-Nrf2-ARE pathway. Annu Rev Pharmacol Toxicol. 2007;47:89–116.
16 Pubchem Bioassay on Compound (CID 5281727). http://pubchem.ncbi.nlm.nih.gov
17 Moon D, McCormack D, McDonald D, McFadden D. Pterostilbene induces mitochondrially derived apoptosis in breast cancer cells in vitro. J Surg Res. 2012;180:208–215.
18 Lin VC, Tsai YC, Lin JN, Fan LL, Pan MH, Ho CT, et al. Activation of AMPK by pterostilbene suppresses lipogenesis and cell-cycle progression in p53 positive and negative human prostate cancer cells. J Agric Food Chem. 2012;60:6399–6407.
19 Chakraborty A, Bodipati N, Demonacos MK, Peddinti R, Ghosh K, Roy P. Long term induction by pterostilbene results in autophagy and cellular differentiation in MCF-7 cells via ROS dependent pathway. Mol Cell Endocrinol. 2012;355:25–40.
20 Zhang W, Sviripa V, Kril LM, Chen X, Yu T, Shi J, et al. Fluorinated N,N-dialkylaminostilbenes for Wnt pathway inhibition and colon cancer repression. J Med Chem. 2011;54:1288–1297.
21 Yang Y, Yan X, Duan W, Yan J, Yi W, Liang Z, et al. Pterostilbene exerts antitumor activity via the notch1 signaling pathway in human lung adenocarcinoma cells. PLoS ONE. 2013;8:e62652.
22 Mena S, Rodríguez ML, Ponsoda X, Estrela JM, Jäättela M, Ortega AL. Pterostilbene-induced tumor cytotoxicity: a lysosomal membrane permeabilization-dependent mechanism. PLoS ONE. 2012;7:e44524.
23 Mosmann T. Rapid colorimetric assay for cellular growth and survival: application to proliferation and cytotoxicity assays. J Immunol Methods. 1983;65:55–63.
24 Tonary AM and Pezacki JP. Simultaneous quantitative measurement of luciferase reporter activity and cell number in two- and three-dimensional cultures of hepatitis C virus replicons. Analy Biochem. 2006;350:239–248.
25 Zhang B, Chen N, Chen HM, Wang ZH, Zheng QS. The critical role of redox homeostasis in Shikonin-induced HL-60 cell differentiation via unique modulation of the Nrf2/ARE pathway. Oxid Med Cell Longev. 2012;2012:781516.
26 Kuang E, Wan Q, Li X, Xu H, Zou T, Qi Y. ER stress triggers apoptosis induced by Nogo-B/ASY overexpression. Exp Cell Res. 2006;312:1983–1988.
27 Cullinan SB, Zhang D, Hannink M, Arvisais E, Kaufman RJ, Diehl JA. Nrf2 is a direct PERK substrate and effector of PERK-dependent cell survival. Mol Cell Biol. 2003;23:7198–7209.
28 Tufekci KU, Bayin EC, Genc S, Genc K. The Nrf2/ARE Pathway: a promising target to counteract mitochondrial dysfunction in parkinson's disease. Parkinson's Disease. 2011;2011: 314082.
29 Neto CC. Cranberry and blueberry: evidence for protective effects against cancer and vascular diseases. Mol Nutr Food Res. 2007;51:652–654.
30 Langcake P, Cornford CA, Pryce RJ. Identification of pterostilbene as a phytoalexin from Vitis vinifera leaves. Phytochemistry. 1979;18:1025–1027.
31 Pubchem Bioassay on Compound (CID 445154). http://pubchem.ncbi.nlm.nih.gov
32 Awale S, Miyamoto T, Linn TZ, Win NN, Tezuka Y, Esumi H, et al. Cytotoxic constituents of Soymida febrifuga from Myanmar. J Nat Prod. 2009;72:1631–1636.
33 Davis AP, Murphy CG, Johnson R, Lay JM, Lennon-Hopkins K, Saraceni-Richards C, et al. The comparative toxicogenomics database: update 2013. Nucleic Acids Res. 2013;41:D1104–D1114.
34 Ovesná Z, Horváthová-Kozics K. Structure-activity relationship of trans-resveratrol and its analogues. Neoplasma. 2005;52:450–455.
35 Ruiz MJ, Fernández M, Picó Y, Mañes J, Asensi M, Carda C, et al. Dietary administration of high doses of pterostilbene and quercetin to mice is not toxic. J Agric Food Chem. 2009; 57:3180–3186.
36 Riche DM, McEwen CL, Riche KD, Sherman JJ, Wofford MR, Dschamp D, et al. Analysis of safety from a human clincial trial with pterostilbene. J toxicol. 2013;2013:463595
37 Roberti M, Pizzirani D, Simoni D, Rondanin R, Baruchello R, Bonora C, et al. Synthesis and biological evaluation of resveratrol and analogs as apoptosis-inducing agents. J Med Chem. 2003;46:3546–3554.
38 Zhang B, Wang XQ, Chen HY, Zheng QS, Li X. The role of

GSH depletion in resvertrol induced HeLa cell apoptosis. IEEE International Conference on Systems Biology (ISB). 2011;1: 8–11.
39 Athar M, Back JH, Tang X, Kim KH, Kopelovich L, Bickers DR, et al. Resveratrol: a review of preclinical studies for human cancer prevention. Toxicol Appl Pharmacol. 2007;224:274–283.
40 Gao X, Xu YX, Divine G, Janakiraman N, Chapman RA, Gautam SC. Disparate in vitro and in vivo antileukemic effects of resveratrol, a natural polyphenolic compound found in grapes. J Nutr. 2002;132:2076–2081.
41 Kimura Y, Okuda H. Resveratrol isolated from Polygonum cuspidatum root prevents tumor growth and metastasis to lung and tumor-induced neovascularization in Lewis lung carcinoma-bearing mice. J Nutr. 2001;131:1844–1849.
42 Kapetanovic IM, Muzzio M, Huang ZH, Thompson TN, McCormick DL. Pharmacokinetics, oral bioavailability, and metabolic profile of resveratrol and its dimethylether analog, pterostilbene, in rats. Cancer Chemoth Pharm. 2010;68:593–601.
43 Schneider JG, Alosi JA, McDonald DE, McFadden DW. Pterostilbene inhibits lung cancer through induction of apoptosis. J Surg Res. 2010;161:18–22.
44 Nutakul W, Sobers HS, Qiu P, Dong P, Decker EA, McClements DJ, et al. Inhibitory effects of resveratrol and pterostilbene on human colon cancer cells: a side-by-side comparison. J Agric Food Chem. 2011;59:10964–10970.
45 Siedlecka-Kroplewska K, Jozwik A, Kaszubowska L, Kowalczyk A, Boguslawski W. Pterostilbene induces cell cycle arrest and apoptosis in MOLT4 human leukemia cells. Folia Histochem Cytobiol. 2012;50:574–580.
46 Mannal P, McDonald D, McFadden D. Pterostilbene and Tamoxifen show an additive effect against breast cancer in vitro. Am J Surg. 2010;200:577–580.
47 Miura T, Muraoka S, Ikeda N, Watanabe M, Fujimoto Y. Antioxidative and prooxidative action of stilbene derivatives. Pharmacol Toxicol. 2000;86:203–208.
48 Rimando AM, Cuendet M, Desmarchelier C, Mehta RG, Pezzuto JM, Duke SO. Cancer chemopreventive and anti-oxidant activities of pterostilbene, a naturally occuring analogue of resveratrol. J Agric Food Chem. 2002;50:3453–3457.
49 Wang XJ, Yang J, Cang H, Zou YQ, Yi J. Gene expression alteration during redox-dependent enhancement of arsenic cytotoxicity by emodin in HeLa cells. Cell Res. 2005;15:511–522.
50 Jeyapaul J, Jaiswal AK. Nrf2 and c-Jun regulation of antioxidant response element (ARE)-mediated expression and induction of gamma-glutamylcysteine synthetase heavy subunit gene. Biochem Pharmacol. 2000;59:1433–1439.
51 Nakagawa T, Zhu H, Morishima N, Li E, Xu J, Yankner BA, et al. Caspase-12 mediates endoplasmic reticulum specific apoptosis and cytotoxicity by amyloid-beta. Nature. 2000;403:98–103.
52 Fischer H, Koenig U, Eckhart L, Tschachler E. Human caspase 12 has acquired deleterious mutations. Biochem Biophys Res Commun. 2002;293:722–726.
53 Hitomi J, Katayama T, Eguchi Y, Kudo T, Taniguchi M, Koyama Y, et al. Involvement of caspase-4 in endoplasmic reticulum stress-induced apoptosis and Abeta-induced cell death. J Cell Biol. 2004;165:347–356.
54 Yamamuro A, Kishino T, Ohshima Y, Yoshioka Y, Kimura T, Kasai A, et al. Caspase-4 directly activates caspase-9 in endoplasmic reticulum stress-induced apoptosis in SH-SY5Y cells. J Pharmacol Sci. 2011;115:239–243.
55 Park JW, Woo KJ, Lee JT, Lim JH, Lee TJ, Kim SH, et al. Resveratrol induces pro-apoptotic endoplasmic reticulum stress in human colon cancer cells. Oncol Rep. 2007;18:1269–1273.
56 Lee HR, Cho JM, Shin DH, Yong CS, Choi HG, Wakabayashi N, et al. Adaptive response to GSH depletion and resistance to L-buthionine-(S,R)-sulfoximine: involvement of Nrf2 activation. Molecular and Cellular Biochemistry. 2008;318:23–31.
57 Chakraborty A, Gupta N, Ghosh K, Roy P. In vitro evaluation of the cytotoxic, anti-proliferative and anti-oxidant properties of pterostilbene isolated from Pterocarpus marsupium. Toxicology in Vitro. 2010;24:1215–1228.
58 Miura H, Takano K, Kitao Y, Hibino S, Choshi T, Murakami R, et al. A carbazole derivative protects cells against endoplasmic reticulum (ER) stress and glutathione depletion. J Pharmacol Sci. 2008;108:164–171.
59 Mačičková T, Pečivová J, Harmatha J, Sviteková K, Nosáľ R. Effect of stilbene derivative on superoxide generation and enzyme release from human neutrophils in vitro. Interdiscip Toxicol. 2012;5:71–75.
60 Hur W, Gray NS. Small molecule modulators of antioxidant response pathway. Curr Opin Chem Biol. 2011;15:162–173.
61 Chiou YS, Tsai ML, Nagabhushanam K, Wang YJ, Wu CH, Ho CT, et al. Pterostilbene is more potent than resveratrol in preventing azoxymethane (AOM)-induced colon tumorigenesis via activation of the NF-E2-related factor 2 (Nrf2)-mediated antioxidant signaling pathway. J Agr Food Chem. 2011;59: 2725–2733.
62 Park EJ, Min HY, Park HJ, Chung HJ, Ahn YH, Pyee JH, et al. Nuclear factor E2-related factor 2-mediated induction of NAD(P)H:quinone oxidoreductase 1 by 3,5-dimethoxy-trans-stilbene. J Pharmacol Sci. 2011;116:89–96.
63 Lushchak V. glutathione homeostasis and functions: potential targets for medical interventions. J Amino Acids. 2012;2012: 736837.
64 Dinkova-Kostova T, Talalay P. NAD(P)H: quinone acceptor oxidoreductase 1 (NQO1), a multifunctional antioxidant enzyme and exceptionally versatile cytoprotector. Arch Biochem Biophys. 2010;501:116–123.
65 Shannon P, Markiel A, Ozier O, Baliga NS, Wang JT, Ramage D, et al. Cytoscape: a software environment for integrated models of biomolecular interaction networks. Genome Res. 2003;13:2498–2504.